

A Series of Red-Light-Emitting Ionic Iridium Complexes: Structures, Excited State Properties, and Application in Electroluminescent Devices

Shu-Juan Liu,^[a] Qiang Zhao,^[a] Qu-Li Fan,^{*[a]} and Wei Huang^{*[a]}

Keywords: Excited states / Iridium / Ionic complexes / Phosphorescence

A series of ionic diiminoiridium complexes $[\text{Ir}(\text{piq}-\text{C}^{\wedge}\text{N})_2(\text{L}-\text{N}^{\wedge}\text{N})](\text{PF}_6)$ were prepared, where $\text{piq}-\text{C}^{\wedge}\text{N}$ is 1-phenylisoquinolinato and $\text{L}-\text{N}^{\wedge}\text{N}$ are bidentate N-coordinating ligands: 2,2'-bipyridine (bpy), 4,4'-dimethyl-2,2'-bipyridine (mbpym), 5,5'-bis(thiopen-2-yl)-2,2'-bipyridine (tbpyt), and 5,5'-bis(9,9-dioctylfluoren-2-yl)-2,2'-bipyridine (FbpyF). X-ray diffraction studies of $[\text{Ir}(\text{piq})_2(\text{mbpym})](\text{PF}_6)$ revealed that the iridium center adopts a distorted octahedral geometry. All complexes exhibited intense and long-lived emission at room temperature. The substituents on the 2,2'-bipyridine moieties influence the photophysical and electrochemical properties. The excited states were investigated through theoretical calculations together with photophysical and

electrochemical properties. It was found that the excited state of the $[\text{Ir}(\text{piq})_2(\text{FbpyF})](\text{PF}_6)$ complex can be assigned to a mixed character of ${}^3\text{LC}$ ($\pi_{\text{N}^{\wedge}\text{N}} \rightarrow \pi^*_{\text{N}^{\wedge}\text{N}}$), ${}^3\text{MLCT}$, ${}^3\text{LLCT}$ ($\pi_{\text{C}^{\wedge}\text{N}} \rightarrow \pi^*_{\text{N}^{\wedge}\text{N}}$), and ${}^3\text{LC}$ ($\pi_{\text{C}^{\wedge}\text{N}} \rightarrow \pi^*_{\text{C}^{\wedge}\text{N}}$). In addition, the alkylfluorene-substituted complex, $[\text{Ir}(\text{piq})_2(\text{FbpyF})](\text{PF}_6)$, had relatively high quantum efficiency and good film-forming ability, and it was expected to be a good candidate for lighting and display applications. A nondoped, single-layer device that incorporates this complex as a light-emitting layer was fabricated and red phosphorescence was obtained.

(© Wiley-VCH Verlag GmbH & Co. KGaA, 69451 Weinheim, Germany, 2008)

Introduction

Iridium (Ir) complexes are explored for a multitude of optoelectronic applications, including lighting, display, and light-emitting electrochemical cells (LEC), because of their high performance.^[1–6] In particular, ionic Ir complexes have emerged as promising chromophoric materials for lighting and display applications according to the reports of recent studies.^[7–15] Inert metal electrodes that are resistant to oxidation in air can be used in these devices and the power consumptions of these devices are low. Further improvement of the stability of these devices can be expected due to the excellent redox stability of charged Ir complexes. Slinker et al.^[7] first demonstrated efficient (luminous power efficiency exceeds 10 lm W^{-1} at just -3 V) yellow electroluminescence from a single-layer device based on an ionic Ir complex. Subsequently, Plummer et al.^[8] investigated the characteristics of electrophosphorescence devices based on ionic Ir complexes and obtained device with high efficiency of 23 cd A^{-1} . Recently, single-layer devices based on ionic Ir complexes emitting green and blue-green light have also been reported.^[9,10] As one of the three primary colors for

full color application, saturated-red emission is indispensable. Therefore, it is especially necessary to fabricate and investigate red-light emitting devices based on ionic Ir complexes.

The photophysical and electrochemical properties of Ir complexes depend on the electronic structures of their ligands and can be manipulated by modifying the chemical structures of the ligands. The excitation properties of Ir complexes have especially experienced a blooming attraction in the past few years, because the species are extremely promising to play the role of active components in organic light-emitting diodes (OLEDs).^[1,16–19] In ionic Ir complexes, both $\text{N}^{\wedge}\text{N}$ and $\text{C}^{\wedge}\text{N}$ coordination are adopted and the excited-state properties of them are very complicated and involve ligand-centered (LC) excited state, metal-to-ligand charge transfer (MLCT) transitions, and Ir–C σ bond-to-ligand charge transfer (SBLCT) transitions. In recent years, density functional theory (DFT) techniques have been receiving large acceptance for their prediction of the ground and excited states in organometallic molecules besides photophysical and electrochemical properties. The application of these approaches would provide the basis for the design of ionic Ir complex light-emitting materials.

In this paper, we prepared a series of red-light-emitting ionic Ir complexes based on 2,2'-bipyridine (bpy) derivatives and 1-phenylisoquinolinato (piq). The molecular structure, theoretical calculation, and photophysical and electrochemical properties were studied. The $\text{piq}-\text{C}^{\wedge}\text{N}$ ligand was selected because it is an appropriate ligand for

[a] Jiangsu Key Lab of Organic Electronics & Information Displays and Institute of Advanced Materials (IAM), Nanjing University of Posts & Telecommunications (NUPT), 66 XinMoFan Road, Nanjing 210003, China
Fax: +86-25-8349 2333
E-mail: wei-huang@njupt.edu.cn

Supporting information for this article is available on the WWW under <http://www.eurjic.org> or from the author.

Ir complexes emitting red light.^[3] The 4,4'-dimethyl-2,2'-bipyridine (mbpym) ligand contains methyl substituents, which are weakly electron donating and are expected to influence the redox and photophysical properties of the corresponding complex. Thiophene substituents on the bpy moiety also might facilitate charge transfer and increase the π -conjugation length of the N[^]N ligand, probably giving rise to a redshift in the emission of the corresponding Ir complex. Alkylfluorene substituents on the bpy ligand are expected to facilitate charge transfer, improve the ability of film formation, and reduce triplet–triplet (T–T) and/or concentration quenching of the corresponding Ir complex. The effects of the ligand structures on the photophysical properties of the complexes were investigated. DFT techniques were applied as approaches to interpret the different behavior of these substituents. The study of the photophysical properties shows that [Ir(piq)₂(FbpyF)](PF₆) (complex 4) is a good candidate for red-light-emitting materials with relatively high quantum efficiency and good film-forming ability. Therefore, we report the first nondoped, single-layer, red-light-emitting OLED by using complex 4 as the active material. Preliminary results indicate that ionic Ir complexes offer promising opportunities in optoelectronic applications.

Results and Discussion

Synthesis and Characterization of the Complexes

The formulas and abbreviations of complexes 1–4 are depicted in Figure 1. 5,5'-Dibromo-2,2'-bipyridine was prepared by classical procedures^[20,21] and oligomer diimine ligands 5,5'-bis(thiopen-2-yl)-2,2'-bipyridine (tbpyt) and 5,5'-bis(9,9-dioctylfluorene-2-yl)-2,2'-bipyridine (FbpyF) were synthesized by Suzuki coupling reactions. All com-

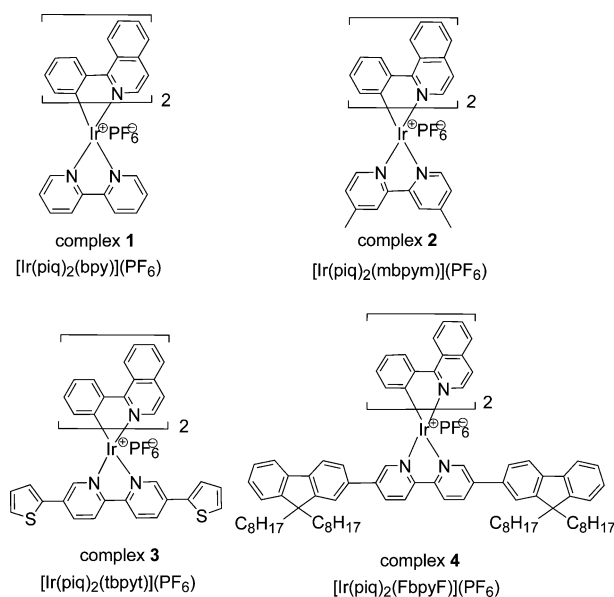


Figure 1. The formulas and abbreviations of the ionic iridium complexes.

plexes were synthesized according to the synthetic routes reported previously.^[6,22–24] The dimeric [Ir(piq)₂(μ -Cl)]₂ precursor prepared as described previously^[25] was used to prepare all the complexes studied here. All complexes were obtained by complexing the chlorido-bridged dimer with the corresponding bidentate N-coordinating ligand under mild conditions in dichloromethane/methanol (3:1). After the reaction was complete, a fivefold excess of potassium hexafluorophosphate was added into the resulting mixture. The complexes were obtained as PF₆⁻ salts. For comparison, complex 1 was also prepared. All complexes obtained were characterized by ¹H NMR spectroscopy, matrix-assisted laser desorption/ionization time-of-flight (MALDI-TOF) mass spectrometry, and elemental analysis. The single-crystal X-ray analysis of complex 2 was also investigated.

Crystal Structure of Complex 2

A single crystal of complex 2 was obtained from an acetonitrile solution by slow evaporation of the solvent, and its structure was investigated by X-ray crystallography analysis. The complex crystallized in the monoclinic *C2/c* space group with centrosymmetric cations and centrosymmetric hexafluorophosphate anions. The perspective drawing of the complex cation is depicted in Figure 2. The coordination of the Ir atom is distorted octahedral and the largest deviation is represented by the bite angle of the bipyridine ligand at 75.8°, which is similar to that found in ionic Ir complexes based on 2,2'-bipyridine reported previously.^[26] The two Ir–C bonds are in a mutually *cis* arrangement, and their high *trans* influence renders slightly longer Ir–N bond lengths in the mbpym ligand [Ir(1)–N(2) and Ir(1)–N(2)#1 2.146(5) Å] than in the cyclometalating ligand [Ir(1)–N(1) and Ir(1)–N(1)#1 2.052(6) Å]. These findings are commonly observed for related cyclometalated Ir complex systems [Ir(C[^]N)₂(L–N[^]N)](PF₆).^[27–31] Probably

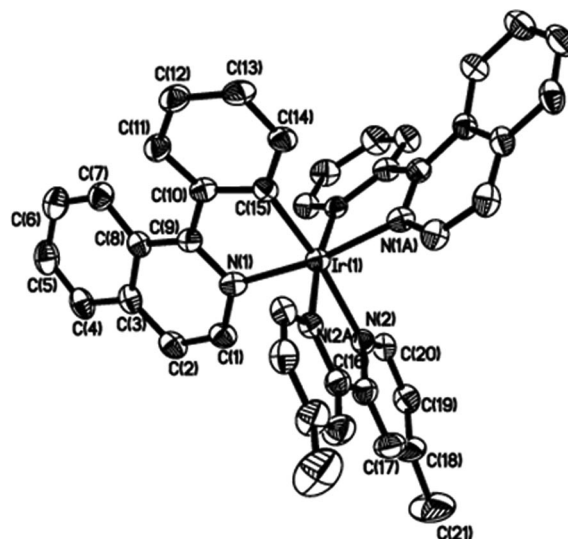


Figure 2. Perspective view of the complex cation of complex 2 with atomic numbering scheme.

because of steric reasons, the two pyridine rings of 2,2'-bipyridine are usually not coplanar.^[28] However, the dihedral angle was only 4.2° in complex **2**, which was significantly smaller than that of other complexes reported,^[28] indicating that bulky groups on the bipyridine would increase the angle.

In the crystal packing, the metal complex cations and PF₆⁻ are connected by weak C–H⋯F–P hydrogen bonds by intra- and intermolecular C–H⋯F interactions involving aromatic or methyl C–H bonds. The average H⋯F distance is about 2.60 Å.

Theoretical Calculations

To further investigate the nature of the excited state, DFT calculations for these complexes were performed. The calculated and experimental geometrical parameters of complex **2** are summarized in Table 1. The overall geometrical parameters of the calculated structures of the complex are in quite good agreement with those of the experimental values from X-ray diffraction. The dihedral angle of the two pyridine rings was also calculated to be 3.7°, which agrees with the corresponding experimental value of 4.2°.

Table 1. Comparison of calculated bond lengths [Å] and angles [°] and experimental values from X-ray diffraction for complex **2**.

	Calculated	Experimental
Ir(1)–C(15)	2.028	1.993(6)
Ir(1)–C(15)#1	2.034	1.993(6)
Ir(1)–N(1)#1	2.175	2.052(6)
Ir(1)–N(1)	2.064	2.052(6)
Ir(1)–N(2)	2.146	2.146(5)
Ir(1)–N(2)#1	2.060	2.146(5)
C(15)–Ir(1)–C(15)#1	86.6	87.7(3)
C(15)–Ir(1)–N(1)#1	96.0	93.2(2)
C(15)#1–Ir(1)–N(1)#1	78.7	79.5(2)
C(15)–Ir(1)–N(1)	79.8	79.5(2)
C(15)#1–Ir(1)–N(1)	97.2	93.2(2)
C(15)–Ir(1)–N(2)#1	97.4	98.5(2)
N(1)#1–Ir(1)–N(1)	175.1	170.0(2)
C(15)–Ir(1)–N(2)	174.1	172.1(2)
C(15)#1–Ir(1)–N(2)	98.4	98.5(2)
N(1)#1–Ir(1)–N(2)	96.1	92.73(19)
N(1)–Ir(1)–N(2)	97.5	95.18(19)
C(15)–Ir(1)–N(2)#1	96.1	98.5(2)
C(15)#1–Ir(1)–N(2)#1	173.8	172.1(2)
N(1)#1–Ir(1)–N(2)#1	97.0	95.18(19)
N(1)–Ir(1)–N(2)#1	98.5	92.73(19)
N(2)–Ir(1)–N(2)#1	77.9	75.8(3)

The distributions of frontier molecular orbitals (HOMO-1, HOMO, LUMO, and LUMO+1) were investigated. All complexes have similar HOMO and LUMO distributions. The HOMO primarily resides on the Ir center and the phenyl groups of the C[^]N ligand. The isoquinolyl groups of the C[^]N ligand also have some contributions to the HOMO. The LUMO is mainly located on the N[^]N ligand. Therefore, the excited states of the complexes can be assigned to the mixed character of MLCT [$d\pi(\text{Ir}) \rightarrow \pi^*_{\text{N}^{\wedge}\text{N}}$]

and LLCT ($\pi_{\text{C}^{\wedge}\text{N}} \rightarrow \pi^*_{\text{N}^{\wedge}\text{N}}$). For complexes **1**, **2**, and **3**, the composition of HOMO-1 is similar to that of HOMO. The LUMO+1 are mainly localized on the isoquinolyl groups of the C[^]N ligands and the phenyl groups of the C[^]N ligands also have some LUMO+1 distribution for complexes **1–4**, showing the possible existence of ³LC ($\pi_{\text{C}^{\wedge}\text{N}} \rightarrow \pi^*_{\text{C}^{\wedge}\text{N}}$) character because of the HOMO (or HOMO-1) → LUMO+1 transitions for complex **1**, **2**, and **3**. For complex **4**, however, the HOMO-1 primarily resides on the fluorene groups of FbpyF instead of the Ir center and the C[^]N ligands. Therefore, the ³LC ($\pi_{\text{N}^{\wedge}\text{N}} \rightarrow \pi^*_{\text{N}^{\wedge}\text{N}}$) character, which is infrequent in other complexes, is possible due to the HOMO-1 → LUMO transitions besides ³MLCT, ³LLCT, and ³LC ($\pi_{\text{C}^{\wedge}\text{N}} \rightarrow \pi^*_{\text{C}^{\wedge}\text{N}}$) characters.

Time-dependent DFT (TDDFT) calculations were then performed to estimate the corresponding transition energy of complex **4**. The calculated parameters for various lower-lying transitions are listed in Table 2. On the basis of Table 2 and UV/Vis absorption spectrum of complex **4** (see Figure 4), it is reasonable to deduce that the major bands at 400–470 nm receive contributions mainly from S₂–S₅, which incorporate mainly a spin-allowed metal–ligand charge transfer (¹MLCT) and a $\pi \rightarrow \pi^*$ intraligand transition. The lowest singlet state, that is, S₁, is obscured in the absorption spectra as a result of the overlap with other bands and the much lower oscillator strength.^[32] Moreover, the lowest triplet state originates from HOMO → LUMO and HOMO → LUMO+1, which apparently possesses a mixed character of ³LC ($\pi_{\text{N}^{\wedge}\text{N}} \rightarrow \pi^*_{\text{N}^{\wedge}\text{N}}$), ³MLCT, ³LLCT ($\pi_{\text{C}^{\wedge}\text{N}} \rightarrow \pi^*_{\text{N}^{\wedge}\text{N}}$), and ³LC ($\pi_{\text{C}^{\wedge}\text{N}} \rightarrow \pi^*_{\text{C}^{\wedge}\text{N}}$). The S₀ → T₁ transition is estimated to be at ca. 687 nm.

Table 2. Calculated singlet and triplet transitions for complex **4**.

State	Excitation	<i>E</i> _{calcd.} [eV]	<i>λ</i> _{calcd.} [nm]	(f)
Singlet Excited State				
1	HOMO → LUMO (98%)	2.15	578	0.0005
2	HOMO-4 → LUMO (2%) HOMO-1 → LUMO (90%)	2.65	467	0.9272
3	HOMO-3 → LUMO (39%) HOMO-2 → LUMO (3%)	2.71	458	0.0147
4	HOMO-3 → LUMO (53%) HOMO → LUMO+1 (53%)	2.73	454	0.0252
5	HOMO-3 → LUMO (6%) HOMO → LUMO+2 (6%) HOMO-3 → LUMO (2%) HOMO → LUMO+1 (4%) HOMO → LUMO+2 (87%)	2.76	449	0.0468
Triplet Excited State				
1	HOMO-1 → LUMO (7%) HOMO → LUMO (89%)	1.81	687	0

Electrochemical Properties

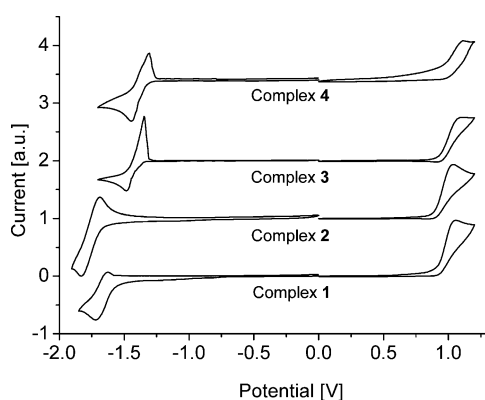
The redox behavior of the ionic Ir complexes was investigated by cyclic voltammetry (CV). The cyclic voltammograms are shown in Figure 3. Complexes **1–4** exhibited an irreversible process upon oxidation. Oxidation processes in Ir cyclometalated compounds have been assigned to metal-

Table 3. Electrochemical properties of complexes **1–4**.^[a]

	E_{red} [V]			ΔE_{p}	E_{ox} [V]		Energy levels [eV]		
	E_{onset}	E_{pc}	E_{pa}		E_{onset}	E_{pa}	HOMO	LUMO	E_{g}
1	-1.58	-1.71	-1.62	0.09	0.91	1.05	-5.71	-3.22	2.49
2	-1.67	-1.83	-1.68	0.15	0.91	1.04	-5.71	-3.13	2.58
3	-1.44	-1.48	-1.35	0.13	0.96	1.11	-5.76	-3.36	2.40
4	-1.49	-1.45	-1.31	0.14	0.96	1.09	-5.76	-3.31	2.45

[a] E_{pa} and E_{pc} are the anodic peak potential and cathodic peak potential, respectively; E_{g} is the bandgap energy; $\Delta E_{\text{p}} = E_{\text{pa}} - E_{\text{pc}}$.

centered orbitals and/or to Ir–C σ -bond orbitals.^[33,34] It is assumed that pure metal-centered oxidation is reversible, and irreversibility increases as the contribution to the HOMO of the cyclometalating phenyl(s) increases.^[35] On such a basis, we assigned the irreversible oxidation processes to orbitals that received a strong contribution from the Ir–C σ -bond orbitals. Upon reduction, a reduction wave and the corresponding reoxidation wave could be observed for each compound. These waves were ascribed to reduction of the diimines instead of piq, as the reduction of the latter is well-known to occur at a more-negative potential.^[28] Therefore, SBLCT [$\sigma(\text{Ir}-\text{C})$ bond $\rightarrow \pi^*(\text{diimine})$] transitions and ³MLCT [$d\pi(\text{Ir}) \rightarrow \pi^*(\text{diimine})$] transitions are possible as well.

Figure 3. Cyclic voltammograms of complexes **1–4**.

According to the onset potentials of the oxidation and reduction of the CV measurements, the HOMO/LUMO energy levels of complexes **1–4** were estimated on the basis of the reference energy level of ferrocene: HOMO/LUMO = $-(4.8 + E_{\text{onset}})$ eV.^[36] The related data are summarized in Table 3. It could be found that the reduction of complex **2** occurred at more-negative potentials and it had a higher LUMO than other complexes probably because of the electron-donating properties of the methyl group. We also found that the energy gap of complex **3** was evidently

smaller than that of other complexes, probably due to the thiophene substituents, which are well-known materials with low energy gaps.

Electronic Absorption

The UV/Vis absorption spectra of complexes **1–4** in air-equilibrated dichloromethane (CH_2Cl_2) solution are shown in Figure 4 and the data are listed in Table 4. For complexes **1** and **2**, the absorption spectra show broad bands from 270 to 600 nm, and the most intense bands are at $\lambda < 300$ nm and moderately intense bands are at longer wavelengths, which extend far within the visible region. The bands between 250 and 300 nm can be assigned to spin-allowed singlet ligand-centered (¹LC) transitions. According to the previous papers, the absorption bands around 350–470 nm are attributed to the spin-allowed singlet charge-transfer (¹CT) transitions.^[37] The absorption features at the lowest energy ($\lambda > 470$ nm) are likely to be assigned to spin-forbidden triplet charge-transfer (³CT) transitions. These singlet-to-triplet transitions become partially allowed, as the presence of the heavy Ir center renders a strong spin-orbit coupling. Unlike complexes **1** and **2**, there are intense absorption bands around 400 nm besides the absorption bands be-

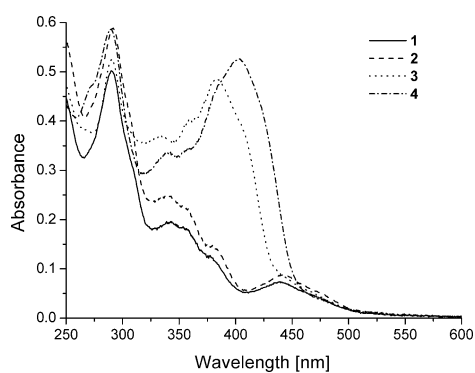
Figure 4. UV/Vis absorption spectra of iridium complexes in CH_2Cl_2 solution at 10^{-5} M.

Table 4. Absorption data of complexes.

Complexes	Absorption wavelengths [nm] (logarithmic absorption coefficients, log [ϵ])
1	290(4.7), 342(4.3), 354(4.3), 378(4.1), 439(3.9), 477(3.6)
2	292(4.8), 340(4.4), 358(4.3), 380(4.2), 442(3.9), 478(3.7)
3	291(4.7), 334(4.6), 359(4.6), 384(4.7), 479(3.6)
4	290(4.8), 341(4.5), 359(4.5), 403(4.7), 479(3.5)

tween 250 and 300 nm that receive contributions mainly from ^1LC involving piq in the absorption spectra of complexes **3** and **4**. They can be attributed to the intense spin-allowed $\pi-\pi^*$ transitions localized on the oligo(bipyridine) units (tbpyt and FbpyF). The visible-region CT bands should be contributed from even SBLCT [$\sigma(\text{Ir}-\text{C})\rightarrow\pi^*(\text{diimine})$] transitions, or simplified piq-to-bpy charge transfer (LLCT) transitions besides Ir-to-bpy MLCT transitions because it has been verified by DFT calculations and electrochemical properties that the HOMO can be significantly delocalized over the cyclometalating ligands, with a large participation also from the Ir-C σ bond orbital for Ir complexes.^[26,38] The absorption characteristics of these complexes are similar to those of related cyclometalated Ir complexes.^[39]

Luminescent Properties

Figure 5 shows the phosphorescence spectra of the Ir complexes observed at 298 and 77 K in different solutions. Upon photoexcitation at 325 nm, complexes **1–4** display intense and long-lived emissions in dilute deaerated CH_2Cl_2 and CH_3CN solutions at room temperature as well as in EtOH/MeOH (4:1) rigid matrix at 77 K. For cyclometalated Ir complexes, in general, phosphorescence mainly originates from ^3LC ($^3\pi-\pi^*$) and ^3CT (including $^3\text{MLCT}$ and $^3\text{LLCT}$) excited states, so the wavefunction of the excited triplet state, Φ_{T} , responsible for phosphorescence is principally expressed as [Equation (1)]:

$$\Phi_{\text{T}} = a\Phi(^3\text{LC})_{\text{T}} + b\Phi(^3\text{CT})_{\text{T}} \quad (1)$$

where a and b are the normalized coefficients and $(^3\text{LC})_{\text{T}}$ and $(^3\text{CT})_{\text{T}}$ are the wavefunctions of the ^3LC and the ^3CT triplet excited states, respectively.^[3] Equation (1) implies that the excited triplet states of the Ir complexes mainly are a mixed character of $(^3\text{LC})_{\text{T}}$ and $(^3\text{CT})_{\text{T}}$.

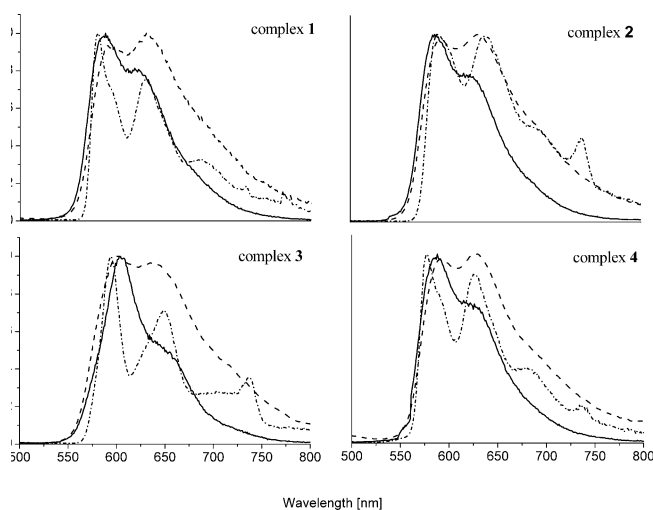


Figure 5. Normalized phosphorescence spectra of the ionic iridium complexes in CH_2Cl_2 (—) and CH_3CN (---) solutions at 298 K and in EtOH/MeOH (4:1) rigid matrix at 77 K (---) excited at 325 nm.

The spectra measured at 298 K of complexes **1–4** are broad structureless bands, which are similar to the character of ^3CT emission state because phosphorescence spectra from the $^3\text{LC}(^3\pi-\pi^*)$ state display vibronic progressions, whereas those from the ^3CT state are broad and featureless according to the previous investigations.^[41,42] In addition, for the phosphorescence spectra at 77 K, well-resolved vibronic progressions between two major peaks are not observed for all complexes studied here. Therefore, the lowest excited states of these complexes are, in a first approximation, probably the ^3CT state. All the data related to the emission spectra of the complexes are summarized in Table 5.

Table 5. Photoluminescence properties of complexes **1–4**.

Complex	Medium (T [K])	$\lambda_{\text{PL,max}}$ [nm]	Φ_{em}	τ [μs]
1	CH_2Cl_2 (298)	587	0.089	0.11
	CH_3CN (298)	588		
	Glass (77)	580		
2	CH_2Cl_2 (298)	585	0.097	2.14
	CH_3CN (298)	594		
	Glass (77)	590		
3	CH_2Cl_2 (298)	604	0.035	1.69
	CH_3CN (298)	601		
	Glass (77)	594		
4	CH_2Cl_2 (298)	588	0.114	2.23
	CH_3CN (298)	591		
	Glass (77)	577		

If $^3\text{MLCT}$ and $^3\text{SBLCT}$ states are emitting states, one would therefore expect that freezing of the solvent and the increase in the solvent polarity should cause obvious blueshifts and redshifts, respectively, in the PL spectra. By lowering the temperature, the rigidity of the medium increases and thus the $^3\text{MLCT}$ and $^3\text{LLCT}$, being less stabilized by the lack of solvent mobility, rise in energy. By increasing the solvent polarity, $^3\text{MLCT}$ and $^3\text{LLCT}$ will be more stable and lower in energy. If the $^3\text{MLCT}$ or $^3\text{SBLCT}$ state is close enough to the ^3LC state, however, a possible inversion of the lowest excited state can be observed upon changing the media. On such a basis, we investigated the PL spectra of complexes reported here at 77 K for comparison. We can find that this shift was much less pronounced (about 10 nm), and there is almost no blueshift in the emission from room-temperature fluid solutions to low-temperature rigid glass suggests that the ^3LC character, which is much less sensitive to changes in the surrounding media, contributes greatly to the excited state of the complexes besides the ^3CT character.^[32–45] A similar behavior was observed for the $[\text{Ir}(\text{ppy})_2\text{bpy}]^+$ complex.^[46] The emission spectra of complexes in CH_3CN solutions at 298 K are shown in Figure 5. The redshift in the PL spectra of complexes **1–4** was not as conspicuous as that reported previously.^[47,48] Thus, as discussed above, it was further indicated that the ^3CT state of the complexes might be close enough to the ^3LC state, and thereby the excited states received much contribution from the ^3CT character mixing strongly with the ^3LC character for complexes **1–4**.^[49]

Substituents on the bipyridine ligand with electron-donating properties may destabilize the π^* orbitals of the diimine ligand, which thereby increases the emission energy of the corresponding complex.^[25] Therefore, we designed and synthesized complex **2**. The emission energy increased slightly relative to that of complex **1**, which was in line with the discussion above, and its emission spectrum showed a very slight blueshift, probably owing to the weak electron-donating properties of the methyl group. The PL spectrum of the Ir complex with thiophene substituents on the diimine ligands (complex **3**) exhibited a redshift relative to that of complex **1**, probably because the thiophene rings lowered the energy level of the π^* orbitals of the diimine ligands as a result of electronic effects. For complex **4**, a relatively high quantum efficiency (Φ_{em}) in comparison to other complexes is realized.^[50] Moreover, complex **4** also exhibited good film-forming ability because of the alkylfluorene substituents. From this, it can be seen that the emission properties of all the complexes studied here agree well with the electrochemical properties and the results we expected initially.

Emission lifetime (τ) monitored at the peak emission was recorded in degassed CH_2Cl_2 solutions at room temperature and analyzed by a single-exponential decay function. The emission lifetimes observed for complexes **1–4** at room temperature fall in the microsecond to submicrosecond range (0.11–2.23 μs) and are significantly reduced in the presence of oxygen, which indicates the phosphorescence nature of the emission.^[27]

Electrophosphorescence of Complex 4

It is noteworthy that the alkylfluorene substituents can reduce T–T and/or concentration quenching, resulting in relatively high quantum efficiency of complex **4**, and the ability of film-forming can be improved as well. In addition, the alkylfluorene substituents will improve the compatibility between complexes and host when the corresponding complexes are used in the host–guest system. Therefore, complex **4** may be a good candidate for use in electrophosphorescent devices.^[51] Here, a single-layer, non-doped device using complex **4** as an emission layer was fabricated by spin-coating, and their properties were investigated. The structure of the device was ITO/complex **4**/Al. The electroluminescence (EL) spectrum is shown in Figure 6, and it exhibits intense broad bands from 600–640 nm. The CIE coordinates ($x = 0.62$ and $y = 0.38$) of the EL emission were evaluated from the EL spectra, and they were in the range of red. To the best of our knowledge, this is the first report of a red phosphorescent OLED that is based on an ionic Ir complex.

The turn-on voltage of the device was 7.8 V. The current density and luminance at 15 V were 589.2 mA cm^{-2} and 94 cd m^{-2} , respectively. The efficiencies of the devices are not satisfying, because the structure of the fabricated device was not optimized; however, the luminance of the red phosphorescence for a single-layer, nondoped device is compar-

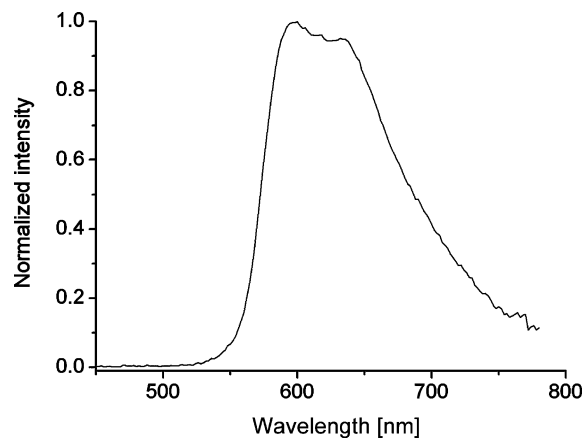


Figure 6. Electroluminescence spectrum of complex **4**. Device structure: ITO/complex **4**/Al.

able to that of related green^[9] and blue-green^[10] emitting devices reported previously. In fact, the factors influencing the performance of devices based on ionic Ir complexes are complicated,^[13] and the investigation of factors influencing the performance of devices based on ionic Ir complexes is an interesting field.^[7–10] Therefore, further studies and optimization of the devices by using these complexes as emission layers are in progress and efficient red-light-emitting devices can be expected.

Conclusions

A series of luminescent cyclometalated diiminoiridium complexes with substituted bipyridine ligands were synthesized, and their theoretical calculations and photophysical and electrochemical properties were investigated. X-ray diffraction studies of complex **2** revealed the coordination of the iridium atom was distorted octahedral. DFT techniques can be applied successfully for the study of the excited state of the complex. This will facilitate the design of new ligands for light-emitting Ir complexes. All complexes exhibited intense and long-lived emission. According to theoretical calculations and electrochemical and photophysical properties, the origin of the emission was assigned to ^3CT mixing strongly with ^3LC transitions. Phosphorescence shifted to red by introducing thiophene substituents onto the bipyridine core. Complex **4** is a good candidate for red-light-emitting materials with relatively high quantum efficiency and good film-forming ability. Preliminary results of a single-layer, nondoped device using complex **4** as an emission layer indicate that ionic Ir complexes offer promising opportunities in optoelectronic applications.

Experimental Section

All manipulations involving air-sensitive reagents were performed under an atmosphere of dry nitrogen. The solvents (THF, toluene) were purified by routine procedures and distilled under an atmosphere of dry nitrogen before use. All reagents, unless otherwise specified, were purchased from Aldrich, Across, and Lancaster and

were used as received. 5,5'-Dibromo-2,2'-bipyridine (**1**) and 9,9-dioctylfluoren-2-boronic acid (**2**) were synthesized as previously described.^[52]

Phenylboronic Acid (3): To a solution of bromobenzene (15.0 g, 0.10 mol) in THF (50 mL) at -78°C was dropwise added *n*-butyllithium (1.6 M in hexane, 65.5 mL, 0.21 mol). After 45 min, trimethyl boronate (24.7 g, 0.24 mmol) was added by syringe. Then, the resulting mixture was warmed to room temperature slowly and stirred overnight. HCl (2 N) was added to the stirred solution whilst the temperature of the solution was maintained at 0°C for 1 h. The organic layer was separated, and the water layer was extracted with diethyl ether (3 \times). The combined ether layer was washed with brine (2 \times) and then dried with anhydrous MgSO_4 . The solvent was evaporated under reduced pressure, and the crude product was slowly dropped into hexane to obtain a white solid (6.51 g, 53%). ^1H NMR (400 MHz, CDCl_3): δ = 8.24 (d, J = 6.8 Hz, 2 H), 7.74 (d, J = 6.8 Hz, 1 H), 7.60 (t, J = 7.2 Hz, 1 H), 7.40–7.53 (m, 3 H) ppm.

1-Phenylisoquinoline (piq) (4): Tetrakis(triphenylphosphane)palladium (0.43 g, 0.37 mmol) was added to a mixture of 1-chloroisoquinoline (1.85 g, 11.50 mmol), **3** (1.4 g, 11.5 mmol), toluene (50 mL), ethanol (25 mL), and an aqueous sodium carbonate solution (2 M, 25 mL) under vigorous stirring. The mixture was stirred at 70°C for 24 h under a nitrogen atmosphere. After cooling to room temperature, the reaction mixture was poured into water and extracted with ethyl acetate. The organic layer was washed with brine several times, and the solvent was then evaporated. The product thus obtained was purified by silica gel column chromatography (hexane/ethyl acetate, 9:1) to yield a white solid (5.0 g, 84%). ^1H NMR (400 MHz, CDCl_3): δ = 8.61 (d, J = 5.6 Hz, 1 H), 8.10 (d, J = 8.4 Hz, 1 H), 7.87 (d, J = 8.4 Hz, 1 H), 7.63–7.72 (m, 4 H), 7.49–7.56 (m, 4 H) ppm. $\text{C}_{15}\text{H}_{11}\text{N}$ (205.25): calcd. C 87.77, H 5.40, N 6.82; found C 87.72, H 5.30, N 6.69.

5,5'-Bis(thiophen-2-yl)-2,2'-bipyridine (5): *n*-Butyllithium (1.6 M in hexane, 23 mL, 74 mmol) was added to a stirred solution of 2-bromothiophene (11.4 g, 70 mmol) in anhydrous diethyl ether (500 mL) at -78°C under a nitrogen atmosphere. After 30 min, trimethyl boronate (10.9 g, 105 mmol) was added. The reaction was stirred at -78°C for 4 h and then warmed to ambient temperature. After 15 h, the reaction was shaken with hydrochloric acid (1.2 N, 200 mL), and the ether phase was separated and extracted with aqueous sodium hydroxide (1 N, 4 \times 50 mL). The combined aqueous phase was then filtered to remove trace amounts of solid and then acidified to pH = 1 at 0°C with concentrated hydrochloric acid. The resulting precipitate was filtered, washed with hydrochloric acid (10^{-2} M), and dried in vacuo to yield the thiophen-2-ylboronic acid as a white powder (7.0 g, 78%). The synthesis method of **5** was similar to that of **4**. ^1H NMR (400 MHz, CDCl_3): δ = 8.95 (m, 2 H), 8.43 (d, J = 8.0 Hz, 2 H), 8.00 (dd, J = 8.4 Hz, J = 2.4 Hz, 2 H), 7.40 (m, 4 H), 7.16 (m, 2 H) ppm. ^{13}C NMR (100 MHz, CDCl_3): δ = 154.31, 146.24, 140.37, 133.70, 130.24, 128.38, 126.16, 124.32, 120.91 ppm. $\text{C}_{18}\text{H}_{12}\text{S}_2\text{N}_2$ (320.43): C 67.47, H 3.77, N 8.74; found C 67.42, H 3.56, N 8.94.

5,5'-Bis(9,9-dioctylfluoren-2-yl)-2,2'-bipyridine (6): The synthesis method was similar to that of **4**. ^1H NMR (400 MHz, CDCl_3): δ = 9.03 (m, 2 H), 8.55 (d, J = 8.4 Hz, 2 H), 8.12 (d, J = 8.4 Hz, 2 H), 7.82 (d, J = 7.6 Hz, 2 H), 7.75 (d, J = 8.0 Hz, 2 H), 7.65 (m, 4 H), 7.36 (m, 6 H), 2.02 (m, 8 H), 1.06–1.2 (m, 40 H), 0.81 (t, J = 7.2 Hz, 12 H), 0.68 (m, 8 H) ppm. ^{13}C NMR (100 MHz, CDCl_3): δ = 154.46, 151.76, 151.01, 147.78, 141.35, 140.39, 136.88, 136.26, 135.12, 127.38, 126.87, 125.88, 122.93, 121.31, 120.87, 120.28, 119.93, 55.23, 40.36, 31.76, 30.01, 29.21, 23.80, 22.60, 14.09 ppm.

$\text{C}_{68}\text{H}_{88}\text{N}_2$ (933.44): C 87.50, H 9.50, N 3.00; found C 87.43, H 9.30, N 2.95.

General Procedure for the Synthesis of Iridium Complexes: $\text{IrCl}_3\cdot 3\text{H}_2\text{O}$ (5.52 mmol) and piq (11.04 mmol) were heated in a 2-ethoxyethanol/water (3:1) under a nitrogen atmosphere. This slurry was heated at 110°C for 24 h. After cooling to room temperature, the precipitate was filtered off and washed with water and ethanol to get red of the solid cyclometalated Ir μ -chlorido-bridged dimer. CH_2Cl_2 and methanol (2:1) were added to the mixture of the cyclometalated Ir μ -chlorido-bridged dimer (0.16 mmol) and N^{^N} ligands (0.32 mmol). The reaction mixture was heated at reflux for 4 h. After cooling to room temperature, a fivefold excess amount of KPF_6 was added, and the mixture was stirred for another 1 h. The solvent was removed, and the solid was dissolved in CH_2Cl_2 again. The precipitate was filtered off and methanol was layered on the filtrate. Red crystal of the complexes can be recrystallized from the solution.

[Ir(piq)₂(bpy)](PF₆): Yield: 80%. ^1H NMR (400 MHz, CDCl_3): δ = 8.94 (m, 2 H), 8.71 (d, J = 8.0 Hz, 2 H), 8.27 (d, J = 8.0 Hz, 2 H), 8.15 (t, J = 8.0 Hz, 2 H), 7.90 (m, 2 H), 7.76 (m, 6 H), 7.37 (m, 6 H), 7.12 (t, J = 8.0 Hz, 2 H), 6.90 (t, J = 7.6 Hz, 2 H), 6.29 (d, J = 7.6 Hz, 2 H) ppm. $\text{C}_{40}\text{H}_{28}\text{F}_6\text{IrN}_4\text{P}$ (901.86): C 53.27, H 3.13, N 6.21; found C 53.15, H 3.24, N 5.96. HRMS (MALDI-TOF): calcd. for $\text{C}_{40}\text{H}_{28}\text{IrN}_4$ [M – PF₆] 756.9; found 755.1.

[Ir(piq)₂(mbpym)](PF₆): Yield: 78%. ^1H NMR (400 MHz, CDCl_3): δ = 8.93 (m, 2 H), 8.57 (s, 2 H), 8.25 (d, J = 8.0 Hz, 2 H), 7.88–7.93 (m, 2 H), 7.73–7.79 (m, 4 H), 7.53 (d, J = 5.6 Hz, 2 H), 7.38 (m, 4 H), 7.10 (m, 4 H), 6.88 (t, J = 7.2 Hz, 2 H), 6.29 (d, J = 6.4 Hz, 2 H), 2.59 (s, 6 H) ppm. $\text{C}_{42}\text{H}_{32}\text{F}_6\text{IrN}_4\text{P}$ (929.91): C 54.25, H 3.47, N 6.02; found C 54.07, H 3.49, N 5.96. HRMS (MALDI-TOF): calcd. for $\text{C}_{42}\text{H}_{32}\text{IrN}_4$ [M – PF₆] 785.2; found 785.9.

[Ir(piq)₂(tbpyt)](PF₆): Yield: 53%. ^1H NMR (400 MHz, CDCl_3): δ = 8.94 (m, 2 H), 8.73 (d, J = 8.8 Hz, 2 H), 8.29 (m, 4 H), 7.93 (m, 2 H), 7.76–7.83 (m, 6 H), 7.48 (d, J = 6.4 Hz, 2 H), 7.40 (d, J = 6.4 Hz, 2 H), 7.34 (d, J = 4.4 Hz, 2 H), 7.21 (t, J = 7.2 Hz, 2 H), 7.12 (m, 2 H), 6.96–7.04 (m, 4 H), 6.34 (d, J = 6.8 Hz, 2 H) ppm. $\text{C}_{48}\text{H}_{32}\text{S}_2\text{F}_6\text{IrN}_4\text{P}$ (1066.11): C 54.08, H 3.03, N 5.26; found C 53.91, H 2.95, N 5.17. HRMS (MALDI-TOF): calcd. for $\text{C}_{48}\text{H}_{32}\text{S}_2\text{IrN}_4$ [M – PF₆] 921.1; found 921.9.

[Ir(piq)₂(Fbpyf)](PF₆): Yield: 66%. ^1H NMR (400 MHz, CDCl_3): δ = 8.99 (m, 2 H), 8.89 (m, 2 H), 8.48 (m, 2 H), 8.37 (d, J = 8.0 Hz, 2 H), 8.06 (m, 2 H), 7.93 (m, 2 H), 7.79 (m, 4 H), 7.70 (m, 4 H), 7.60 (m, 2 H), 7.32–7.44 (m, 10 H), 7.25 (m, 2 H), 7.12 (s, 2 H), 6.99 (t, J = 7.6 Hz, 2 H), 6.43 (d, J = 7.6 Hz, 2 H), 1.96 (m, 8 H), 1.02 (m, 40 H), 0.77 (t, J = 7.2 Hz, 12 H), 0.51 (m, 8 H) ppm. $\text{C}_{98}\text{H}_{108}\text{F}_6\text{IrN}_4\text{P}$ (1679.11): C 70.01, H 6.48, N 3.34; found C 69.79, H 6.69, N 3.24. HRMS (MALDI-TOF): calcd. for $\text{C}_{98}\text{H}_{108}\text{IrN}_4$ [M – PF₆] 1534.2; found 1534.5.

UV/Vis absorption spectra were recorded with a Shimadzu 3000 UV/Vis/NIR spectrophotometer. NMR spectra were recorded with a Mercury Plus 400 MHz NMR spectrometer. Elemental analyses were performed with a Vario EL III O-Element Analyzer system. MALDI-TOF experiments were carried out by using a Shimadzu AXIMA-CFRM plus matrix-assisted laser desorption/ionization time-of-flight mass spectrometer (Kratos Analytical, Manchester, U. K.). Photoluminescence spectra were measured with an Edinburgh FLS920 fluorescence spectrophotometer. Emission lifetime was recorded with a single-photon counting spectrometer from Edinburgh Instruments (FLS920) with a hydrogen-filled pulse lamp as the excitation source. The data were analyzed by iterative convolution of the luminescence decay profile with the instrument re-

sponse function by using software package provided by Edinburgh Instruments. Emission quantum yield measurements were carried out at room temperature in a CH_2Cl_2 solution of 10^{-5} M (degassed by several freeze–pump–thaw cycles) by using quinine sulfate in aerated 1.0 N H_2SO_4 ($\Phi = 0.546$) as the standard solution. Cyclic voltammetry was performed with an Eco chemie's Autolab. It was conducted at room temperature in a typical three-electrode cell with a working electrode (glassy carbon electrode), a reference electrode [Ag/Ag^+ , referenced against ferrocene/ferrocenium (FOC)], and a counter electrode (Pt wire) under a nitrogen atmosphere at a sweeping rate of 100 mV s^{-1} in a solution of 0.1 M tetra-*n*-butylammonium hexafluorophosphate (Bu_4NPF_6) in acetonitrile. The onset potentials were determined from the intersection of two tangents drawn at the rising current and background current of the cyclic voltammogram. A single crystal of complex **2** was mounted on a glass fiber and transferred to a Bruker SMART CCD area detector. Crystallographic measurement was carried out by using a Bruker SMART CCD diffractometer, σ scans, graphite-monochromated Mo- K_α radiation ($\lambda = 0.71073 \text{ \AA}$) at room temperature. The structure was solved by direct methods and refined by full-matrix least-squares on F^2 values by using the program SHELXS-97.^[53] All non-hydrogen atoms were refined anisotropically. Hydrogen atoms were calculated in ideal geometries. For the full-matrix least-squares refinements [$I > 2\sigma(I)$], the unweighted and weighted agreement factors of $R_1 = \Sigma(F_o - F_c)/\Sigma F_o$ and $wR_2 = [\Sigma w(F_o^2 - F_c^2)^2/\Sigma wF_o^4]^{1/2}$ were used. The device configuration was ITO/complex **4** (3000 rpm, 1 min)/Al. The device was fabricated by spinning the emissive layer on the top of the ITO, and subsequently the metallic top electrode was evaporated in a home-built evaporation chamber. The concentration of complex **4** in toluene was 3 mg mL^{-1} . CCDC-288897 contains the supplementary crystallographic data for this paper. These data can be obtained free of charge from The Cambridge Crystallographic Data Centre via www.ccdc.cam.ac.uk/data_request/cif.

Supporting Information (see footnote on the first page of this article): HOMO and LUMO distributions of complexes **1–4**.

Acknowledgments

This work was financially supported by the Nanjing University of Posts and Telecommunications under Grant NY206070 as well as the National Natural Science Foundation of China under Grants 60235412, 50428303, 90406021, 20574012, and 20774043.

- [1] A. B. Tamayo, S. Garon, T. Sajoto, P. I. Djurovich, I. M. Tsyba, R. Bau, M. E. Thompson, *Inorg. Chem.* **2005**, *44*, 8723–8732.
- [2] I. R. Laskar, T.-M. Chen, *Chem. Mater.* **2004**, *16*, 111–117.
- [3] A. Tsuboyama, H. Iwawaki, M. Furugori, T. Mukaide, J. Kamatani, S. Igawa, T. Moriyama, S. Miura, T. Takiguchi, S. Okada, M. Hoshino, K. Ueno, *J. Am. Chem. Soc.* **2003**, *125*, 12971–12979.
- [4] I. R. Laskar, S.-F. Hsu, T.-M. Chen, *Polyhedron* **2005**, *24*, 189–200.
- [5] C. Adachi, M. A. Baldo, M. E. Thompson, S. R. Forrest, *J. Appl. Phys.* **2001**, *90*, 5048–5051.
- [6] S. Lamansky, P. Djurovich, D. Murphy, F. Abdel-Razzaq, R. Kwong, I. Tsyba, M. Bortz, B. Mui, R. Bau, M. E. Thompson, *Inorg. Chem.* **2001**, *40*, 1704–1711.
- [7] J. D. Slinker, A. A. Gorodetsky, M. S. Lowry, J. Wang, S. Parker, R. Rohl, S. Bernhard, G. G. Malliaras, *J. Am. Chem. Soc.* **2004**, *126*, 2763–2767.
- [8] E. A. Phummer, A. Dijken, H. W. Hofstraat, L. D. Cola, K. Brunner, *Adv. Funct. Mater.* **2005**, *15*, 281–289.
- [9] M. S. Lowry, J. I. Goldsmith, J. D. Slinker, R. Rohl, R. A. Pascal Jr., G. G. Malliaras, S. Bernhard, *Chem. Mater.* **2005**, *17*, 5712–5719.
- [10] J. D. Slinker, C. Y. Koh, G. G. Malliaras, *Appl. Phys. Lett.* **2005**, *86*, 173506-1–173506-3.
- [11] J. Slinker, D. Bernards, P. L. Houston, H. D. Abruña, S. Bernhard, G. G. Malliaras, *Chem. Commun.* **2003**, *19*, 2392–2399.
- [12] A. A. Gorodetsky, S. Parker, J. D. Slinker, D. A. Bernards, M. H. Wong, G. G. Malliaras, S. Flores-Torres, H. D. Abruña, *Appl. Phys. Lett.* **2004**, *84*, 807–809.
- [13] D. A. Bernards, T. Biegala, Z. A. Samuels, J. D. Slinker, G. G. Malliaras, S. Flores-Torres, H. D. Abruña, J. A. Rogers, *Appl. Phys. Lett.* **2004**, *84*, 3675–3677.
- [14] D. A. Bernards, J. D. Slinker, G. G. Malliaras, S. Flores-Torres, H. D. Abruña, *Appl. Phys. Lett.* **2004**, *84*, 4980–4982.
- [15] J. D. Slinker, J. Rivnay, J. S. Moskowitz, J. B. Parker, S. Bernhard, H. D. Abruña, G. G. Malliaras, *J. Mater. Chem.* **2007**, *17*, 2976–2988.
- [16] I. Sokolik, R. Priestley, A. D. Walser, R. Dorsinville, C. W. Tang, *Appl. Phys. Lett.* **1996**, *69*, 4168–4170.
- [17] M. A. Baldo, C. Adachi, S. R. Forrest, *Phys. Rev. B* **2000**, *62*, 10967–10977.
- [18] J. M. Lupton, I. D. W. Samuel, M. J. Frampton, R. Beavington, P. L. Burn, *Adv. Funct. Mater.* **2001**, *11*, 287–294.
- [19] F. Neve, M. L. Deda, A. Crispini, A. Bellusci, F. Puntoriero, S. Campagna, *Organometallics* **2004**, *23*, 5856–5863.
- [20] P. F. H. Schwab, F. Fleischer, J. Michl, *J. Org. Chem.* **2002**, *67*, 443–449.
- [21] G. R. Newkome, A. K. Patri, E. Holder, U. S. Schubert, *Eur. J. Org. Chem.* **2004**, 235–254.
- [22] F. Neve, A. Crispini, S. Serroni, F. Loiseau, S. Campagna, *Inorg. Chem.* **2001**, *40*, 1093–1101.
- [23] S. Campagna, G. Denti, S. Serroni, M. Ciano, V. Balzani, *Inorg. Chem.* **1991**, *30*, 3728–3732.
- [24] K. Dedeian, P. I. Djurovich, F. O. Garces, G. Carlson, R. J. Watts, *Inorg. Chem.* **1991**, *30*, 1685–1687.
- [25] A. B. Tamayo, B. D. Alleyne, P. I. Djurovich, S. Lamansky, I. Tsyba, N. N. Ho, R. Bau, M. E. Thompson, *J. Am. Chem. Soc.* **2003**, *125*, 7377–7387.
- [26] M. Lepeltier, T. K.-M. Lee, K. K.-W. Lo, L. Toupet, H. L. Bozec, V. Guerschais, *Eur. J. Inorg. Chem.* **2005**, 110–117.
- [27] F. A. Cotton, C. A. Murillo, H.-C. Zhou, *Inorg. Chem.* **2000**, *39*, 1039–1041.
- [28] K. K.-W. Lo, D. C.-M. Ng, C.-K. Chung, *Organometallics* **2001**, *20*, 4999–5001.
- [29] K. K.-W. Lo, C.-K. Chung, D. C.-M. Ng, N. Zhu, *New J. Chem.* **2002**, *26*, 81–88.
- [30] K. K.-W. Lo, C.-K. Chung, T. K.-M. Lee, L.-H. Lui, K. H.-K. Tsang, N. Zhu, *Inorg. Chem.* **2003**, *42*, 6886–6897.
- [31] R. Urban, R. Krämer, S. Mihan, K. Polborn, B. Wagner, W. Beck, *J. Organomet. Chem.* **1996**, *517*, 191–200.
- [32] H.-C. Li, P.-T. Chou, Y.-H. Hu, Y.-M. Cheng, R.-S. Liu, *Organometallics* **2005**, *24*, 1329–1335.
- [33] P. Didier, I. Ortmans, A. K.-D. Mesmaeker, R. J. Watts, *Inorg. Chem.* **1993**, *32*, 5239–5245.
- [34] S. Serroni, A. Juris, S. Campagna, M. Venturi, G. Denti, V. Balzani, *J. Am. Chem. Soc.* **1994**, *116*, 9086–9091.
- [35] G. Calogero, G. Giuffrida, S. Serroni, V. Ricevuto, S. Campagna, *Inorg. Chem.* **1995**, *34*, 541–545.
- [36] M. S. Liu, J. D. Luo, A. K.-Y. Jen, *Chem. Mater.* **2003**, *15*, 3496–3500.
- [37] F. Lafolet, S. Welter, Z. Popović, L. D. Cola, *J. Mater. Chem.* **2005**, *15*, 2820–2828.
- [38] M. Polson, S. Fracasso, V. Bertolasi, M. Ravaglia, F. Scandola, *Inorg. Chem.* **2004**, *43*, 1950–1956.
- [39] E. A. Plummer, J. W. Hofstraat, L. D. Cola, *Dalton Trans.* **2003**, 2080–2084.
- [40] Q. Zhao, S.-J. Liu, M. Shi, C.-M. Wang, M.-X. Yu, L. Li, F.-Y. Li, T. Yi, C.-H. Huang, *Inorg. Chem.* **2006**, *45*, 6152–6160.

- [41] S. Lamansky, P. Djurovich, D. Murphy, F. Abdel-Razzaq, H.-E. Lee, C. Adachi, P. E. Burrows, S. R. Forrest, M. E. Thompson, *J. Am. Chem. Soc.* **2001**, *123*, 4304–4312.
- [42] P. Spellane, R. J. Watts, A. Vogler, *Inorg. Chem.* **1993**, *32*, 5633–5636.
- [43] J.-P. Collin, I. M. Dixon, J.-P. Sauvage, J. A. G. Williams, F. Barigelletti, L. Flamigni, *J. Am. Chem. Soc.* **1999**, *121*, 5009–5016.
- [44] M. Licini, J. A. G. Williams, *Chem. Commun.* **1999**, *19*, 1943–1944.
- [45] W. Goodall, J. A. G. Williams, *J. Chem. Soc., Dalton Trans. Trans.* **2000**, *17*, 2893–2895.
- [46] M. G. Colombo, A. Hauser, H. U. Guedel, *Inorg. Chem.* **1993**, *32*, 3088–3092.
- [47] P. M. Griffiths, F. Loiseau, F. Puntoriero, S. Serroni, S. Campagna, *Chem. Commun.* **2000**, 2297–2298.
- [48] K. K.-W. Lo, C.-K. Chung, D. C.-M. Ng, N. Zhu, *Chem. Eur. J.* **2003**, *9*, 475–483.
- [49] M. G. Colombo, T. C. Brunold, T. Riedner, H. U. Güdel, M. Förtsch, H.-B. Bürgi, *Inorg. Chem.* **1994**, *33*, 545–550.
- [50] H. Z. Xie, M. W. Liu, O. Y. Wang, X. H. Zhang, C. S. Lee, L. S. Hung, S. T. Lee, P. F. Teng, H. L. Kwong, H. Zheng, C. M. Che, *Adv. Mater.* **2001**, *13*, 1245–1248.
- [51] K. R. J. Thomas, J. T. Lin, H.-M. Lin, C.-P. Chang, C.-H. Chuen, *Organometallics* **2001**, *20*, 557–563.
- [52] S.-J. Liu, Q. Zhao, R.-F. Chen, Y. Deng, Q.-L. Fan, F.-Y. Li, L.-H. Wang, C.-H. Huang, W. Huang, *Chem. Eur. J.* **2006**, *12*, 4351–4361.
- [53] G. M. Sheldrick, *SHELXTL-Plus V5.1 Software Reference Manual*, Bruker AXS Inc., Madison, **1997**.

Received: November 3, 2007

Published Online: March 27, 2008

(Since its publication in Early View, a few minor changes have been made.)